# Bone remodeling analysis of the humerus after resurfacing and stemless shoulder arthroplasties

Beatriz Ferreira dos Santos*

Instituto Superior Técnico, Lisboa, Portugal
*e-mail: beatrizfdsantos@tecnico.ulisboa.pt

**ABSTRACT**

Although the shoulder arthroplasty has undergone evident advances over the last years, several complications still limit its success. New implant designs, such as resurfacing and stemless implants, have been developed to improve the long-term outcomes of shoulder arthroplasty and to provide an improved bone quality in revision operations. However, it is well known from Wolff's law that the introduction of an implant into the bone changes its natural load distribution, leading to a significant reduction in bone mass, which can compromise the long-term stability of the implant. The aim of the present study is to analyse the bone remodelling process of the humerus after resurfacing and stemless shoulder arthroplasties using three-dimensional finite element models. The 3D geometric model of the humerus was generated from the Visible Human Project data. The resurfacing and stemless implants were modelled in Solidworks. The bone remodelling model applied is based on a global optimization criterion that considers both structural stiffness and the metabolic cost of bone maintenance. The loading condition considered comprised 6 load cases related to different positions of abduction in the frontal plane and anterior flexion in the sagittal plane. The forces applied, which included muscle forces and the reaction force at the shoulder joint, were estimated by a multibody model of the upper limb. The bone remodelling simulations were performed considering a healthy condition and a poor bone quality condition. The results were analysed qualitatively and quantitatively by comparing the bone density distribution obtained for the humerus without an implant to that obtained for the implanted humerus. The results showed similar levels of bone resorption for the resurfacing and stemless implants. Nevertheless, the stemless implant lost less density at the implant fixation, which suggests that the stemless implants may be better supported in the long-term, and thus could lead to a better outcome than the resurfacing implants. For the poor bone quality condition, the loss of bone increased, which supports the limited performance of these implants for reduced bone stock.

**Keywords:** Shoulder joint, shoulder arthroplasty, stemless implant, resurfacing implant, bone remodeling, finite element method.

## 1. Introduction

The shoulder joint replacement by an implant, commonly referred as shoulder arthroplasty, is an effective treatment for several shoulder pathologies and has demonstrated positive clinical outcomes over the years. However, it is associated with a set of complications that may compromise its long term performance. Of particular concern regarding the humeral component are component loosening and periprosthetic fracture complications (Bohsali et al., 2017). Although the reason behind these complications is not yet fully understood, studies on the hip and shoulder suggest that the implant's stability can be affected by stress shielding. This phenomenon is characterized by an adaptation of bone as a result of changes in the distribution of load due to the insertion of the implant (Nagels et al., 2003; Quental et al., 2012).

Bearing in mind that shoulder arthroplasty has become an option not only for a population with a higher average life expectancy, but also for younger and more active patients, new implants have been developed to improve the long term outcomes of shoulder arthroplasty and to provide ease of revision with improved bone quality, if needed. In order to reduce humeral stem complications, progressive shortening of the stem along with cementless application techniques have been developed (Churchill & Athwal, 2016). Over the last few years, resurfacing humeral implants have gained popularity by allowing the preservation of the majority of the humeral head, with minimal bone resection; however, with difficult exposure for glenoid replacement (Burgess et al., 2009; Churchill & Athwal, 2016; Schmidutz et al., 2014). Short- and medium-term studies demonstrate positive functional results, but it is known from the hip that resurfacing implants also affect the distribution of natural bone loading, inducing stress shielding (Gupta et al., 2006; Ong et al., 2006; Schmidutz et al., 2014). Stemless humeral implants emerged with the aim of completely avoiding stem-related complications while maintaining an optimal bone quality in revision surgeries and providing an

optimal access for glenoid replacement (Churchill & Athwal, 2016).

Finite element models are a type of biomechanical models that have been widely used to study the effect of load transfer in bone morphology by estimating the changes in stress and strain distributions (Poelert et al., 2013). Due to the high computational cost associated with FE analyses, models are usually simplified by focusing only on a specific part of the human body (Favre et al., 2009). Regarding the shoulder joint, most studies have investigated the biomechanics of the scapula, since one of the major complications of the total shoulder arthroplasty is the loosening of the glenoid component (Bohsali et al., 2017; Zheng et al., 2017). In the literature, few studies with finite element models address resurfacing and stemless shoulder arthroplasties, and only recently has the phenomenon of stress shielding been evaluated by assessing the difference in bone deformation before and after a shoulder arthroplasty with two different resurfacing implants (Schmidutz et al., 2014). Although the existence of stress shielding has been demonstrated, the bone adaptation process was not effectively modelled. Moreover, a single load condition was considered without the action of muscle forces, which certainly affected the characterization of the mechanical environment of the bone. Despite there is still reduced information available regarding a comprehensive assessment of stemless implants, Razfar et al. (2015) compared the proximal humeral stresses between three different stem length implants; they found that reducing the stem length may decrease stress shielding of the proximal bone, leading to a better mimicking of the intact bone. Favre & Henderson (2016) have evaluated the micromotion of a stemless humeral implant during several upper limb activities in order to assess the primary stability of the implant.

Bone remodelling models have been used to simulate the bone adaptation to the mechanical environment using finite element models. Although most simulations have focused on the hip and knee (Behrens et al., 2009; P. R. Fernandes et al., 2002; Geraldes et al., 2016; Quilez et al., 2017; Ruben et al., 2012), recently they have also been applied to the shoulder joint in both scapula (Quental, Fernandes, et al., 2014; Sharma et al., 2010; Sharma & Robertson, 2013; Suárez et al., 2012) and humerus (Quental et al., 2012). Although the adaptation process of the humerus with stemmed cemented and cementless implants has been addressed by Quental et al. (2012), as far as the author knows, there are no studies evaluating the bone remodelling process in resurfacing and stemless implants of the shoulder joint. In the hip, the resurfacing implants have been already assessed regarding the bone adaptation simulation (Behrens et al., 2009; Gupta et al., 2006; Rothstock et al., 2011).

The purpose of this study is to investigate the process of bone remodelling of the humerus in the presence of resurfacing and stemless implants using three-dimensional finite element models. Six load cases, related to different positions of abduction in the frontal plane and flexion in the sagittal plane are considered, including muscle forces and the reaction force at the shoulder joint. Furthermore, a poorer bone condition is also considered to investigate the effect of bone quality on the adaptation process.

## 2. Material and methods

### 2.1 Computational modelling

The 3D geometric model of the proximal right humerus was generated from the CT images of the Visible Human Project data (Spitzer et al., 1996). The resurfacing and stemless implants were modelled in Solidworks®, based on the Global C.A.P.™ Resurfacing Humeral Head Implant from DePuy and on the Sidus™ Stem-Free Shoulder from Zimmer, respectively (DePuy, 2004; Zimmer, 2012). Henceforth, the modelled implants, depicted in Figure 1, will be simply referred to as Global CAP and Sidus. Afterwards, the shoulder arthroplasty was virtually simulated in Solidworks® for the two implants. The implant positioning was approved by an orthopaedic surgeon.

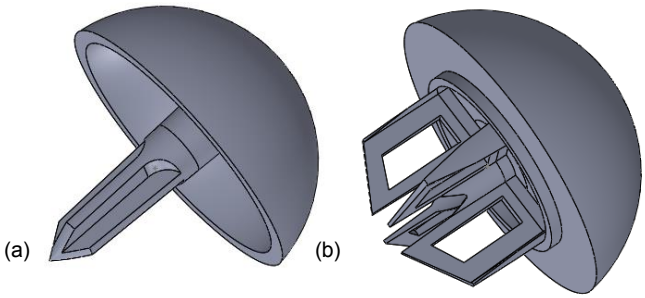


**Figure 1** Geometric models of global CAP, in (a), and sidus, in (b).

The finite element meshes of the humerus and the implants were created in Abaqus® 6.14 using linear tetraheadral elements. The intact humerus, implanted humeral head and humeral diaphysis were meshed with an element average length of 2, 1.5 and 3 mm, respectively. All the components of the implants were meshed with an element average length of 2 mm. Figure 2 presents the finite element meshes generated for the intact and implanted bones and for the different implants modelled.

The head of both implants is made of a Cobalt-Chromium alloy (CoCrMo), while the stem in the Global CAP and the anchor in Sidus are made of a titanium alloy ($TiAl_6V_4$). All of the structures of the implants were considered homogeneous, isotropic and linear elastic. The Young's moduli considered for CoCrMo and $TiAl_6V_4$ were 230 and 115 GPa, respectively, whereas the Poisson's ratio was considered 0.3 for both materials (Quental et al., 2012). The material properties of bone result from the solution of the optimization problem that integrates the finite element method with a numerical simulation of the process of bone adaptation,

assuming a Poisson's ratio of 0.3 and a Young's modulus of 18 GPa for compact bone (Gupta & Dan, 2004; Quental et al., 2012; Quental, Folgado, et al., 2014).

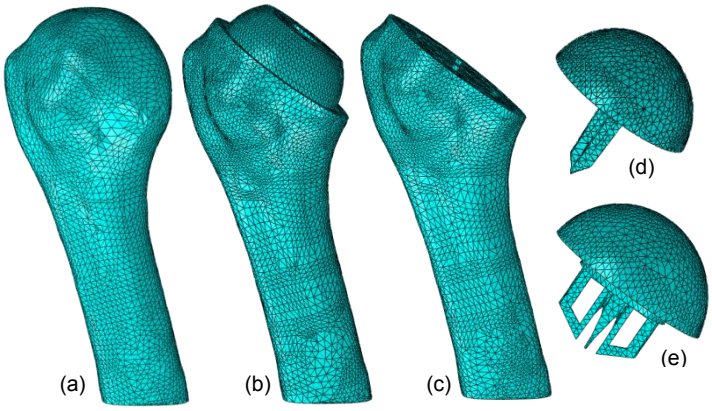


**Figure 2** Anterior view of the finite element meshes. (a) Intact bone; Implanted bone with the (b) Global CAP implant and the (c) Sidus implant; (d) Global CAP implant; (e) Sidus implant.

Considering an idealized condition of full osteointegration, the interaction between the head's undersurface of the Global CAP implant and the anchor of Sidus and the corresponding bone surface was considered rigidly bonded. Contact was defined between the distal stem of the Global CAP and the bone, and between the bone and the rim of both implants in contact with bone, considering friction coefficients of 0,36 (Eberle & Augat, 2007) and 0,26 (Sobocinski, 2015), respectively.

In order to properly characterize the mechanical environment of bone, the action of 11 muscle forces responsible for the appropriate functioning of the humerus within the shoulder complex were considered, including the Supraspinatus, Subscapularis, Pectoralis Major, Latissimus Dorsi, Teres Major, Deltoid, Coracobrachialis, Infraspinatus, Teres Minor, Biceps brachii and Triceps brachii muscles.

Six different load cases were applied to the model. These include muscle and joint reaction forces at 10º, 60º and 110º of arm abduction in the frontal plane and anterior flexion in the sagittal plane. The data regarding the magnitude of muscle and glenohumeral joint reaction forces was acquired using the multibody musculoskeletal model of the upper limb developed by Quental (2013), which is based on the same subject whose humerus is here analysed. The muscle and joint reaction forces applied to the humerus are presented in Table 1.

The muscle forces were applied on attachment points located in the centroid of each muscle site, which was defined directly on the bone surface. The attachment points are independent of the mesh, being able to transfer force to the model through the definition of *coupling* constraints (Dassault, 2012). These constrains connect the attachment points to the corresponding nodes of the muscle sites, as shown in Figure 3.

Regarding the glenohumeral joint reaction forces, they were also applied in attachment points; however, instead of defining the connected nodes in Abaqus®, an algorithm was developed in Matlab® to select all the surface humeral head nodes within a circular region centred at the force application point. The force applied at the attachment point was distributed by the coupling nodes through a uniform and quadratic weighting methods for the muscle and glenohumeral joint forces, respectively. The lower extremity of the humerus was fixed by an *encastre* condition, which constrains all displacements and rotations (Dassault, 2012).

**Table 1** Muscle and joint reaction forces, in N, for the six load conditions at 10º, 60º and 110º of arm abduction and anterior flexion. The forces are in the global coordinate system of the right humerus described in this work.

| | | Abduction | | | Flexion | | |
|---|---|---|---|---|---|---|---|
| Muscle | Direction | 10º | 60º | 110º | 10º | 60º | 110º |
| Pectoralis major | X | -6.9 | 0.0 | -8.9 | -11.7 | 0.0 | 0.0 |
| | Y | 4.0 | 0.0 | -2.7 | 3.3 | 0.0 | -0.5 |
| | Z | 6.2 | 0.0 | 4.3 | 8.3 | 0.0 | 0.2 |
| Latissimus dorsi | X | 0.0 | 0.0 | 0.0 | 0.0 | 0.0 | 0.0 |
| | Y | 0.0 | 0.0 | 0.0 | 0.0 | 0.0 | 0.0 |
| | Z | 0.0 | 0.0 | 0.0 | 0.0 | 0.0 | 0.0 |
| Deltoid | X | -3.2 | -21.1 | -16.3 | -3.9 | -116.8 | -94.0 |
| | Y | 4.4 | 43.1 | 41.8 | 5.6 | 67.5 | 44.5 |
| | Z | 33.4 | 153.2 | 140.9 | 12.5 | 183.4 | 134.2 |
| Subscapularis | X | 0.0 | 0.0 | 0.0 | 0.0 | -2.3 | 5.7 |
| | Y | 0.0 | 0.0 | 0.0 | 0.0 | -42.3 | -26.9 |
| | Z | 0.0 | 0.0 | 0.0 | 0.0 | 63.7 | 120.5 |
| Supraspinatus | X | -2.7 | -6.6 | 10.3 | -14.2 | -7.1 | 0.0 |
| | Y | -20.6 | -59.9 | -10.0 | -44.9 | -12.0 | 0.0 |
| | Z | 26.7 | 86.5 | 96.6 | 59.1 | 19.7 | 0.0 |
| Infraspinatus | X | 2.5 | -3.9 | -14.8 | 10.4 | 19.9 | 2.3 |
| | Y | -22.6 | -107.3 | -79.9 | -56.4 | -94.6 | -6.3 |
| | Z | 9.1 | 67.4 | 97.6 | 19.3 | 73.2 | 15.1 |
| Teres major | X | 0.0 | 0.0 | 0.0 | 0.0 | 0.0 | 0.0 |
| | Y | 0.0 | 0.0 | 0.0 | 0.0 | 0.0 | 0.0 |
| | Z | 0.0 | 0.0 | 0.0 | 0.0 | 0.0 | 0.0 |
| Teres minor | X | 0.0 | 0.0 | -0.4 | 0.0 | 3.1 | 3.5 |
| | Y | 0.0 | 0.0 | -9.3 | 0.0 | -11.4 | -24.4 |
| | Z | 0.0 | 0.0 | 8.5 | 0.0 | 7.6 | 53.8 |
| Coracobrachialis | X | 0.0 | 0.0 | 0.0 | 0.0 | 0.0 | 0.0 |
| | Y | 0.0 | 0.0 | 0.0 | 0.0 | 0.0 | 0.0 |
| | Z | 0.0 | 0.0 | 0.0 | 0.0 | 0.0 | 0.0 |
| Biceps brachii | X | 15.8 | 20.8 | 0.0 | 46.3 | 0.0 | 0.0 |
| | Y | -5.2 | -23.9 | 0.0 | -19.3 | 0.0 | 0.0 |
| | Z | -4.6 | -15.0 | 0.0 | -12.9 | 0.0 | 0.0 |
| Triceps brachii | X | 0.0 | 0.0 | 11.7 | 0.0 | 0.0 | 10.8 |
| | Y | 0.0 | 0.0 | -4.9 | 0.0 | 0.0 | -4.6 |
| | Z | 0.0 | 0.0 | -14.6 | 0.0 | 0.0 | -13.5 |
| Glenohumeral joint | X | 17.0 | 61.4 | 55.1 | 12.6 | 49.8 | 28.5 |
| | Y | 65.8 | 200.6 | 93.0 | 175.0 | 185.3 | 52.8 |
| | Z | -11.3 | -277.4 | -362.1 | -36.3 | -381.2 | -342.6 |

## 2.2 Bone remodeling model

The bone remodelling model applied in this work was developed by Fernandes et al. (1999), who proposes a three-dimensional optimization model for bone adaptation.

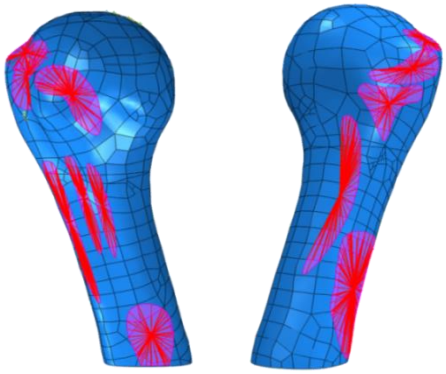

**Figure 3** Muscle sites where the six load cases were applied. The coupling interactions are also illustrated. On the left side the muscles presented are: Supraspinatus, Subscapularis, Pectoralis Major, Latissimus Dorsi, Teres Major, Biceps brachii and Coracobrachialis (Anterior view). On the right side the muscles presented are: Supraspinatus, Infraspinatus, Teres Minor, Deltoid and Triceps brachii (Posterior view).

The model considers bone as a linearly elastic orthotropic porous material with a periodic microstructure. The microstructure is obtained by the repetition of cubic unit cells with rectangular holes, known as open cell (Folgado et al., 2004), with dimensions $a_1$, $a_2$ and $a_3$. These dimensions allow the simulation of different levels of porosity. At each point, bone is characterized through a local microstructure, as shown in Figure 4, in which its relative density and orientation are defined by the parameters $\boldsymbol{a} = [a_1, a_2, a_3]^T$ and by the Euler angles $\boldsymbol{\theta} = [\theta_1, \theta_2, \theta_3]^T$, respectively. The relative density is given by $\rho = 1 - a_1a_2 - a_1a_3 - a_2a_3 + 2a_1a_2a_3$, with $a_i \in [0,1]$ and $i = 1,2,3$.

Mathematically, the process of bone adaptation is defined as the minimization of the structural compliance, thus maximizing the structural stiffness, while taking into account the metabolic cost associated with bone tissue maintenance.

The law of bone remodelling is expressed as:

$$\sum_{P=1}^{NC}\left[-\alpha^P \int_\Omega \frac{\partial E^H_{ijkl}(\boldsymbol{a},\boldsymbol{\theta})}{\partial \boldsymbol{a}} \varepsilon_{ij}(\boldsymbol{u}^P)\varepsilon_{kl}(\boldsymbol{v}^P)\, d\Omega\right] + k\int_\Omega m\rho^{m-1}\frac{\partial \rho}{\partial \boldsymbol{a}} = 0 \quad (1)$$

$$\sum_{P=1}^{NC}\left[-\alpha^P \int_\Omega \frac{\partial E^H_{ijkl}(\boldsymbol{a},\boldsymbol{\theta})}{\partial \boldsymbol{\theta}} \varepsilon_{ij}(\boldsymbol{u}^P)\varepsilon_{kl}(\boldsymbol{v}^P)\, d\Omega\right] = 0, \quad (2)$$

where NC is the number of applied loads, $\alpha^P$ are the load weight factors satisfying $\sum_{P=1}^{NC}\alpha^P = 1$, $\Omega$ is the volume occupied by the bone structure, $E^H_{ijkm}$ are the homogenized material properties, $\varepsilon_{ij}$ and $\varepsilon_{kl}$ are the components of the strain field, $\boldsymbol{u}^P$ is the set of displacements field and $\boldsymbol{v}^P$ to the set of virtual displacements. The parameters $k$ and $m$ allow the adjustment of the model to different biological factors such as age, hormone status and disease. Both of them play an important role in the bone remodelling model, since the optimal bone mass will rely heavily on their value (Quental, 2013). The parameter $k$ represents the metabolic cost per unit of bone volume. Accordingly, an increase in $k$ is associated with a bone structure that presents lower bone mass, since the bone homeostasis maintenance cost to the organism is higher. The parameter $m$ represents a corrective factor for the preservation of intermediate densities. Hence, an increase in $m$ corresponds to an increase of the intermediate density regions, mitigating the formation of regions with extreme densities (Quental, Folgado, et al., 2014).

The load weight factors $\alpha^P$ were defined according to the relative frequencies of each movement (abduction and flexion) and arm positions during daily activities. For the arm elevations of 10º, 60º and 110º, they were 0.231504, 0.077910, 0.008586 for abduction and 0.496496, 0.167090, 0.018414 for flexion, respectively (Coley et al., 2008, 2009). The bone remodelling model was evaluated at the nodes, following a node-based approach and with a step length $s$ of 10. The apparent density of bone, $\rho_{ap}$ is related to the relative density, $\rho$ by the expression $\rho_{ap}(kg\ m^{-3}) = 1800\,\rho$, to the extent that $1800\ kg\ m^{-3}$ is considered the maximum bone apparent density of cortical bone.

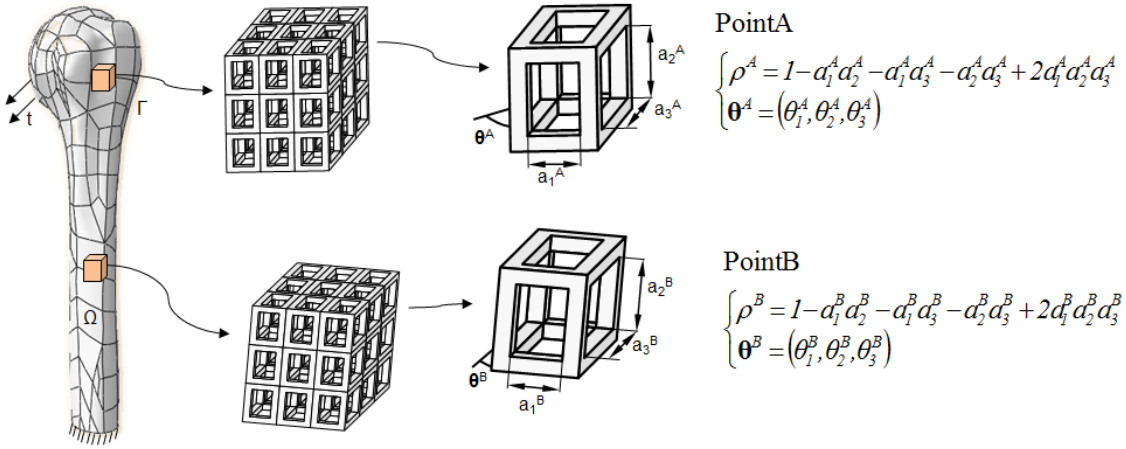


**Figure 4** Material model of bone (Quental, 2013)

#### 2.2.1 Validation of the bone remodelling model for the intact bone

The finite element model of the intact humerus was used to validate the bone remodelling model, i.e., to understand to what extent the model could successfully reproduce the actual bone density distribution of the subject under analysis. For that, different values for the parameter $k$, ranging from $0.1 \times 10^{-4}$ to $0.5 \times 10^{-3}$, and the parameter $m$, ranging from 3 to 6, were evaluated to assess which combination of these parameters results in the nearest qualitative solution to the CT images. For comparison purposes, all simulations were performed for 300 iterations. In order to start the bone remodelling simulation from a more accurate solution, the density values of bone were estimated from the CT images used to create the geometric model of humerus.

#### 2.2.2 Bone remodelling of the humerus after the shoulder arthroplasty

The bone remodelling simulations were performed considering a healthy condition and a poor bone quality condition. For a healthy condition, the bone remodelling analyses for each model of the implanted bone were performed using the $k$ and $m$ parameters selected in the validation of the bone remodelling model with the intact bone. A poor bone quality condition of bone was also assessed by considering a higher cost of bone maintenance. Based on the results reported by Santos et al. (2010), the parameter $k$ was defined 4.7 times larger than that of the healthy condition. The simulations were performed for 300 iterations.

The initial bone material properties were defined using the final density distribution of the bone remodelling simulation of the intact humerus, for each condition of bone. That way, the simulation starts from a more realistic condition.

### 2.3 Evaluation of the results

#### 2.3.1 Validation of the bone remodelling model for the intact bone

The resulting bone density distributions were evaluated, qualitatively, by visual comparison with the CT images and, quantitatively, by comparing the bone relative density values from the bone remodelling analyses with the real relative density values from the CT images, based on a statistical analysis (Quental, Folgado, et al., 2014). The root-mean-square (RMS) error between these was calculated based on an absolute and relative difference, $\Delta\rho_a$ and $\Delta\rho_r$, respectively, expressed as:

$$\Delta\rho_a = \left|\rho_i^{REM} - \rho_i^{CT}\right| \tag{3}$$

$$\Delta\rho_r = \left|\frac{\rho_i^{REM} - \rho_i^{CT}}{\rho_i^{CT}}\right| \tag{4}$$

where, $\rho_i^{REM}$ and $\rho_i^{CT}$ represent the bone relative densities of node $i$ resulting from the bone remodelling analyses and the CT images, respectively. The mean and standard deviation (SD) of bone density distribution were also computed, for each bone remodelling analysis.

Due to the design of the implants modelled, the humeral head is the most important region. Therefore, the RMS error, mean and SD were computed only for the humeral head up to the surgical neck.

#### 2.3.2 Bone remodelling of the humerus after the shoulder arthroplasty

In order to evaluate how bone adapts in the presence of an implant, qualitative and quantitative comparisons were evaluated. For the qualitative analysis, the absolute difference in bone relative density was assessed between the final and the initial solutions of the bone remodelling analyses for the implanted bone.

For the quantitative analysis, the proximal region of the humerus was divided into twelve and eight regions of interest, ROI, for the implanted bone with Global CAP and Sidus, respectively, as depicted in Figures 5 and 6 (Schmidutz et al., 2014). The number of regions is different for the two implanted bones because of their difference in design. Nonetheless, the first eight regions are comparable for both implants.

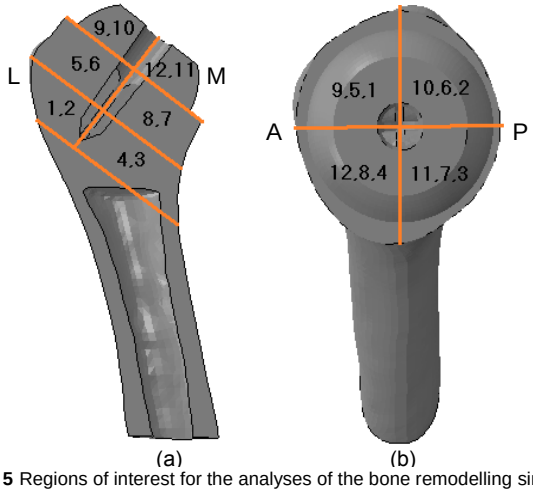


**Figure 5** Regions of interest for the analyses of the bone remodelling simulations of the implanted humerus with Global CAP: (a) anterior view, and (b) medial view.

The change in bone mass, calculated for each ROI, is given by

$$\Delta m(\%) = \frac{\sum_{i=1}^{n}(\rho_i^{final} - \rho_i^{initial}) \times \mathrm{V}_i}{\sum_{i=1}^{n}\rho_i^{initial} \times \mathrm{V}_i} \times 100 \tag{5}$$

where $n$ is the total number of nodes within the ROI under analysis, $\rho_i^{final}$ and $\rho_i^{initial}$ are the bone relative densities of node $i$ ($i \in ROI$) at the end and beginning of the bone remodelling simulation, respectively, and $\mathrm{V}_i$ is the volume associated to the node $i$ (Quental, Fernandes, et al., 2014). The computation of the change in bone mass for each ROI allows a better perception of the local behaviour of bone in relation to its formation and resorption.

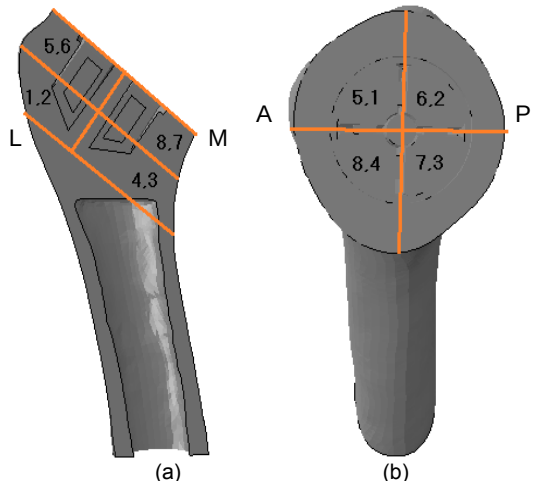


**Figure 6** Regions of interest for the analyses of the bone remodelling simulations of the implanted humerus with Sidus: (a) anterior view, and (b) medial view.

## 3. Results

### 3.1 Validation of the bone remodelling model for the intact bone

The RMS errors of the absolute and relative differences ($\Delta\rho_a$ and $\Delta\rho_r$, respectively) between the relative density of the bone remodelling analyses and the CT images are presented in Table 2, along with the mean and SD. For all simulations, the 300 iterations led to a solution that was changing less than 0.008% in volume, between consecutive iterations.

The best solutions, i.e., the solutions with the lowest RMS errors, are characterized by the parameter $k$ of $5 \times 10^{-5}$ and the parameter $m$ of 4 and 5, for the absolute and relative differences, respectively. It should be noted, nonetheless, that other solutions present comparable errors, and thus would also be suitable options. The mean and standard deviation (SD) of the CT images' relative densities are 0.5946 and 0.1731, respectively. Considering these measures for the bone remodelling solutions, presented in Table 2, it can be observed that the optimal mean density value stands for the parameters $k$ and $m$ of $5 \times 10^{-5}$ and 4, respectively, with a mean value of 0.5977 and SD of 0.1684. Thereby, this solution is deemed as the most suitable to reproduce the bone density distribution of the analysed humerus.

The qualitative comparison between the bone remodelling solution considered as the best and the CT images is presented in Figure 7. For the sake of briefness, only three horizontal slices are shown. Although differences exist between the images, the results are in general consistent and represent a reasonable approximation of the actual bone density.

### 3.2 Bone remodelling of the humerus after the shoulder arthroplasty

The absolute changes in the bone relative density, with respect to the initial condition of the bone remodelling analyses, are illustrated in Figure 8, for the implanted bone with the Global CAP and the Sidus considering healthy and poor bone quality conditions. For all simulations, the 300 iterations led to a solution that was changing less than 0.02% in volume, between consecutive iterations. The process of bone adaptation is categorized into bone apposition, equilibrium, and bone resorption. The equilibrium condition was considered for absolute variations in bone density smaller than 0.04.

**Table 2** RMS error of $\Delta\rho_a$ and $\Delta\rho_r$ between the bone relative density of the bone remodelling analyses and the CT images; and mean and standard deviation of the performed bone remodelling analyses.

| $m$ | $k$ | RMS error | | Mean (SD) |
|---|---|---|---|---|
| | | $(\Delta\rho_a)$ | $(\Delta\rho_r)$ | |
| 3 | $1 \times 10^{-5}$ | 0.0870 | 0.1579 | 0.6421 (0.1816) |
| | $5 \times 10^{-5}$ | 0.0802 | 0.1378 | 0.5864 (0.1775) |
| | $1 \times 10^{-4}$ | 0.1117 | 0.1794 | 0.5299 (0.1681) |
| | $2 \times 10^{-4}$ | 0.1779 | 0.2754 | 0.4550 (0.1504) |
| | $3 \times 10^{-4}$ | 0.2220 | 0.3415 | 0.4095 (0.1396) |
| | $5 \times 10^{-4}$ | 0.2737 | 0.4204 | 0.3565 (0.1265) |
| 4 | $1 \times 10^{-5}$ | 0.0878 | 0.1601 | 0.6446 (0.1791) |
| | $5 \times 10^{-5}$ | 0.0782 | 0.1344 | 0.5977 (0.1684) |
| | $1 \times 10^{-4}$ | 0.0991 | 0.1522 | 0.5515 (0.1533) |
| | $2 \times 10^{-4}$ | 0.1503 | 0.2169 | 0.4903 (0.1320) |
| | $3 \times 10^{-4}$ | 0.1861 | 0.2662 | 0.4530 (0.1195) |
| | $5 \times 10^{-4}$ | 0.2299 | 0.3302 | 0.4080 (0.1064) |
| 5 | $1 \times 10^{-5}$ | 0.0888 | 0.1624 | 0.6469 (0.1775) |
| | $5 \times 10^{-5}$ | 0.0781 | 0.1365 | 0.6080 (0.1629) |
| | $1 \times 10^{-4}$ | 0.0907 | 0.1397 | 0.5703 (0.1457) |
| | $2 \times 10^{-4}$ | 0.1293 | 0.1796 | 0.5201 (0.1231) |
| | $3 \times 10^{-4}$ | 0.1586 | 0.2160 | 0.4885 (0.1106) |
| | $5 \times 10^{-4}$ | 0.1957 | 0.2663 | 0.4499 (0.0971) |
| 6 | $1 \times 10^{-5}$ | 0.0897 | 0.1644 | 0.6488 (0.1767) |
| | $5 \times 10^{-5}$ | 0.0789 | 0.1408 | 0.6168 (0.1601) |
| | $1 \times 10^{-4}$ | 0.0858 | 0.1366 | 0.5857 (0.1421) |
| | $2 \times 10^{-4}$ | 0.1141 | 0.1582 | 0.5446 (0.1195) |
| | $3 \times 10^{-4}$ | 0.1376 | 0.1834 | 0.5179 (0.1069) |
| | $5 \times 10^{-4}$ | 0.1692 | 0.2220 | 0.4842 (0.0934) |

The changes in bone mass for the regions of interest of the implanted bone with the Global CAP and Sidus, described in detail in Figures 5 and 6, are presented in Table 3, for both healthy and reduced quality bones. Note that, for each ROI, values above zero indicate an increase in the bone mass whereas values below zero indicate a decrease. The global percentages of the regions 1 to 4, 5 to 8, and 9 to 12 represent the change in bone mass for the set of ROI. The ROI total-8 and total-12, in Table 3, represent the change in bone mass for all the 8 and 12 regions under analysis.

Considering the healthy condition, the Global CAP implanted bone shows a high level of bone resorption in the proximal humerus, as illustrated in Figure 8 (a), indicating unloaded bone stock due to the presence of the implant. Bone apposition is mainly seen below the outer rim and below the tip of the stem of the

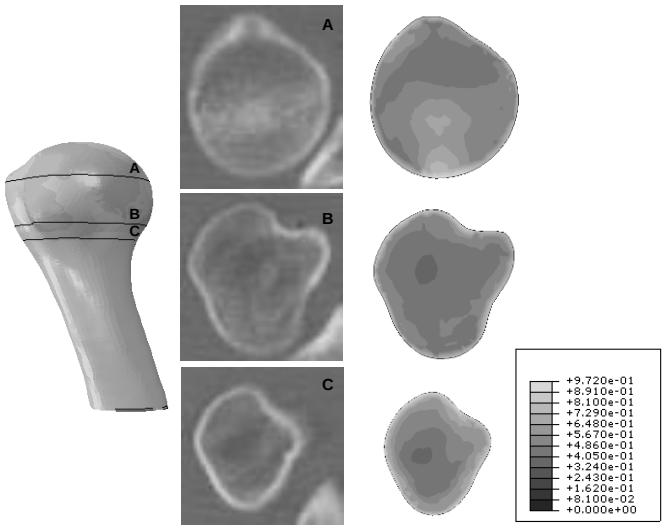


**Figure 7** Comparison between the CT images, on the left, and the bone remodelling result, on the right, for the parameters $k$ and $m$ of $5 \times 10^{-5}$ and 4, respectively.

implant. This suggests that, after the prosthesis implantation, the load is transferred predominantly through that region. The Sidus implanted bone, depicted in Figure 8 (b), shows some bone resorption in the central region, where the anchor is placed. Bone apposition occurs mainly at the interface between the bone and the head of the implant, around the medial and inferior segments of the anchor and at the end of the anchorage open-fins, on the anterior and posterior sections. Quantitatively, the results are quite similar for the common regions of the two implanted humerus in the healthy condition, as it can be seen in Table 3. A global decrease in bone mass of 0.3% and 0.8% is seen in regions 1 to 4, for the Global CAP and Sidus implanted bones, respectively. With respect to regions 5 to 8, both implants lead to similar decreases in bone mass, of 3.8%. Nonetheless, the highest decreases in bone mass occur in regions 9 to 12 of the Global CAP implanted bone, with a global reduction of 12.8%.

The results obtained for a poorer condition of bone are qualitatively similar to those obtained for a healthy condition. However, the level of bone resorption increased compared to that of the healthy condition, as depicted in Figure 8. As expected, considering the quantitative analysis, the results are worse for the bone with reduced quality in comparison to the normal condition, for each implanted bone, as shown in Table 3.

## 4 Discussion

Recently, new implant designs have been developed to improve the long-term outcomes of shoulder arthroplasty and to provide an improved bone quality in revision operations. In the literature, there is still insufficient information regarding the effect of stress shielding in the humerus when resurfacing and stemless implants are implanted. Moreover, the bone remodelling process with respect to resurfacing and stemless shoulder arthroplasties

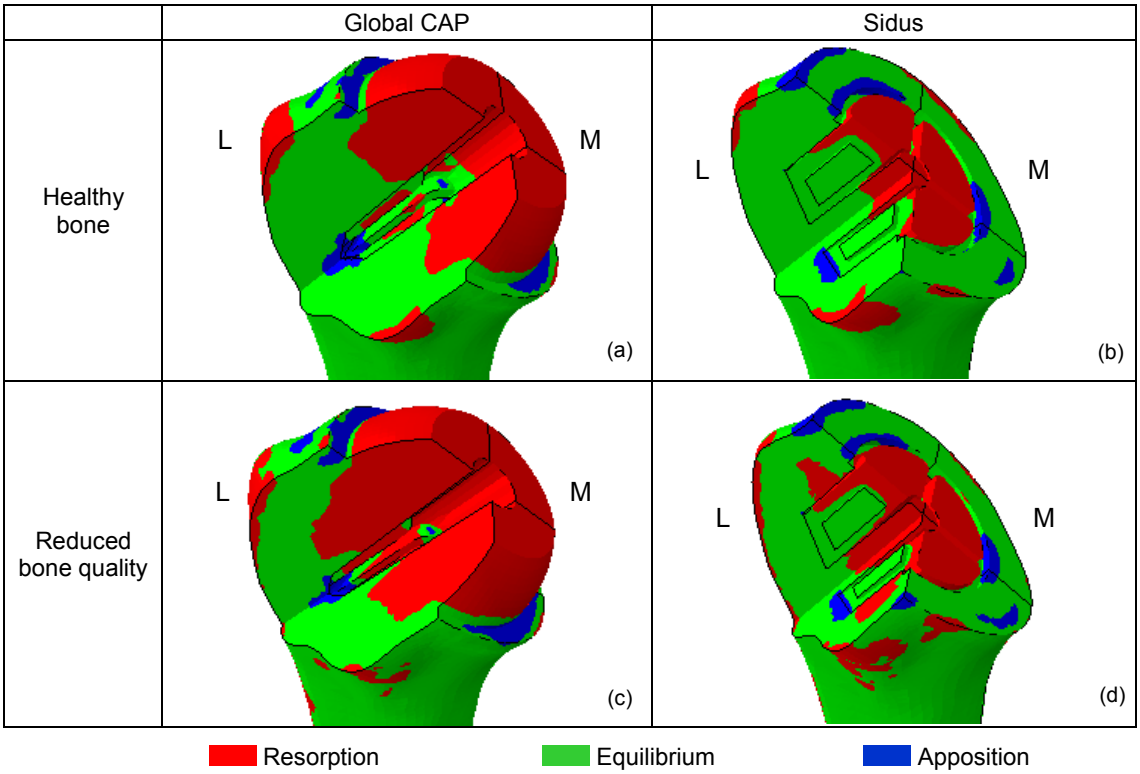


**Figure 8** Absolute changes in bone relative density, with respect to the initial condition of the bone remodelling analyses, of the implanted bone with Global CAP and Sidus, considering healthy and poor bone quality conditions (anterior view).

**Table 3** Changes in bone mass, in percentage, with respect to the initial condition of the bone remodelling analyses, for the ROI of the implanted bone with the Global CAP and Sidus, for both healthy and reduced quality bones. Darker shaded cells denote a higher decrease of bone mass.

| ROI | Healthy bone | | | | Reduced bone quality | | | |
|---|---|---|---|---|---|---|---|---|
| | Global CAP | | Sidus | | Global CAP | | Sidus | |
| 1 | -1.95 | -0.30 | -2.81 | -0.76 | -5.33 | -3.31 | -6.60 | -3.91 |
| 2 | 0.44 | | 0.03 | | -3.25 | | -3.63 | |
| 3 | -0.11 | | -1.05 | | -2.31 | | -3.80 | |
| 4 | 0.01 | | 0.26 | | -2.98 | | -2.49 | |
| 5 | -6.35 | -3.79 | -6.41 | -3.77 | -11.22 | -8.03 | -10.58 | -8.02 |
| 6 | -2.78 | | -4.35 | | -7.61 | | -8.46 | |
| 7 | -4.31 | | -2.75 | | -7.79 | | -7.43 | |
| 8 | -1.69 | | -1.47 | | -5.40 | | -5.51 | |
| 9 | -12.85 | -12.84 | | | -25.42 | -25.99 | | |
| 10 | -13.69 | | | | -28.11 | | | |
| 11 | -12.81 | | | | -24.94 | | | |
| 12 | -12.02 | | | | -25.49 | | | |
| Total-8 | -2.23 | | -2.29 | | -5.93 | | -5.99 | |
| Total-12 | -4.46 | | | | -10.13 | | | |

has not been addressed in previous studies. Therefore, three-dimensional finite element models of the humerus were developed in this study, to analyse the bone remodelling process after the virtual implantation of a resurfacing implant and a stemless implant. The influence of the initial bone quality was also evaluated.

This work focused on the comparison of the bone density distribution obtained for the humerus without an implant to that obtained for the implanted humerus. The qualitative results obtained show similar levels of bone resorption for the resurfacing and stemless implants around the stem and central region of the anchor, respectively. In particular, for the Global CAP implant, decreased bone density is observed in the region underlying the resurfaced head, indicating unloaded bone stock due to the presence of the implant. On the other hand, bone apposition is observed around the outer rim of the implants and below the tip of the stem and anchorage fins, for the resurfacing and stemless implants, respectively. Quantitatively, the results are in accordance with the qualitative results, confirming a higher decrease in bone mass at the proximal region of the humerus. This reduction in the proximal bone mass is greater for the Global CAP implant, since the head is not resected and the loads are transferred through the outer shell of the implant, leading to unloaded bone stock below the implant's cap. Bone resorption decreased from the proximal to the distal part of the humeral head.

The surgical technique recommends implanting these types of prostheses only in the presence of bone with good quality (DePuy, 2004; Zimmer, 2012). The results obtained for the poor bone quality condition show an increased loss of bone at the fixation site, which might compromise the stability of the implant. In other words, the results support the recommendations of manufacturers given the limited performance of these implants for poor bone quality conditions.

Although the results confirm the incidence of stress shielding after the implantation of both prostheses, the stemless implant lost less density at the implant fixation, suggesting that, when seeking for a better support of the implant with satisfactory bone quality, stemless implants may lead to superior long-term outcomes when compared with the resurfacing implants.

The results obtained in this work for the resurfacing implant are consistent with a previous study conducted by Schmidutz et al. (2014) which evaluated stress shielding using FE analysis and bone remodelling pattern of two different shoulder resurfacing implant designs retrieved in vivo. The implant designs evaluated on that study have two different fixation methods: a central stem and a conical crown shaped ring. The results show similar pattern of stress shielding in the FE and retrieval analyses. The stress shielding is induced by an inhomogeneous pattern of strain distribution after implantation; however, for the conical crown shaped ring the results appeared more homogenous, presenting a more balanced strain pattern around the stem. The authors suggest that the use of stems that transfer the load not only to the center of bone, but also to the adjoining area might reduce the amount of unloaded bone, which is in accordance with the results obtained in the present study for the stemless implant. Also, for the models with reduced bone quality, the effect of stress shielding was in general 2-3 times higher compared to the model with a normal bone quality, which is in line with the current study. In other study, Razfar et al. (2015) investigated the effect of the implant stem length on the proximal bone stresses. Although reductions in stem length resulted in cortical bone stresses that better mimicked the proximal intact cortical bone, significantly increased stresses in proximal trabecular bone were identified for the stemless model. This happens because all the joint reaction force is transferred across the metaphyseal region where the implant is secured. Nonetheless, they considered the stemless design as the better option to mimic the intact bone after the joint replacement, although with concern about its stability.

Adequate primary stability of the implant is fundamental to guarantee the long-term success of uncemented stemless shoulder implants (Favre & Henderson, 2016). Although recent short-term follow-up studies of stemless implants have shown promising results (Churchill, 2014; Churchill & Athwal, 2016), there are no long-term studies addressing the potential outcome of stemless implants. Given that implant's design affects the local bone

adaptation process, the results of a single implant should not be generalized to others. As far as the authors know, there are no clinical data available regarding the stemless implant considered in this study, neither computation models evaluating the stress shielding effect in the humerus after the shoulder arthroplasty.

Computational models addressing the effects of stress shielding have largely been applied to the hip resurfacing arthroplasty and the results seem to agree with the current work (Behrens et al., 2009; Gupta et al., 2006; Ong et al., 2006; Pal & Gupta, 2011). In the remodelling process of a cemented hip resurfacing arthroplasty, Gupta et al. (2006) described bone density reductions between 60% and 90% in the region below the resurfaced head, indicating significant bone resorption, whereas bone apposition was described around the distal tip of the implant. Also, from the proximal to the distal end of the implant, bone resorption was reduced to a maximum of 10%. Although the majority of hip resurfacing studies focus on cement fixation, some biomechanical studies have evaluated the uncemented type of fixation (Ong et al., 2006; Pal & Gupta, 2011). Ong et al. (2006) found no differences in bone remodelling between cemented and cementless hip resurfacing implants, under comparable interface conditions. Moreover, their work found increased stress around the stem which induced bone formation, while reduced stress was described underneath the resurfacing head which led to bone resorption. Pal & Gupta (2011) reported bone density reductions and increases around 50-80% in the region underlying the resurfaced head and around the distal tip of the stem, respectively, for cementless hip resurfacing implants. Although the results described are consistent with those obtained in this work, these must be evaluated with caution since the mechanical environment and the forces acting on the hip and shoulder joints are different.

The present study overcomes some limitations of the work of Schmidutz et al. (2014). In particular, the bone adaptation process was effectively modelled to understand the effect of the resurfacing and stemless prostheses on the humerus. Six load conditions, including the action of muscle forces were considered to better characterize the mechanical environment of the bone. Additionally, this study is strengthened by the evaluation of the bone remodelling process after a stemless shoulder arthroplasty, which was never considered before by means of computational simulation.

Regardless of its contribution, this work is not without limitations. First of all, the bone geometry and density distribution were based on CT-scan data of a single representative humerus, so further studies on a subject-specific basis would be valuable. The definition of the muscle sites was based on the Atlas of Human Anatomy (Netter, 2006), aided by personal perception, and therefore susceptible to inaccuracies. The present study was strengthened by the use of 6 load cases but the application of more load cases may improve the bone remodelling simulations. The osteointegration process was not modelled. Idealized conditions of complete osteointegration were considered. Since it was not possible to obtain the physical models of the implants, these were modelled according to the surgical techniques (DePuy, 2004; Zimmer, 2012). Thus, some variations with respect to the original design may exist. The significant differences in the design of each implant made the comparison between them difficult to perform. For instance, although the approach to define the regions of interest was the same in both cases – i.e., the regions were defined using the cruciform shape of the stem and anchor, for the resurfacing and stemless implants, respectively –, the defined regions of interest (1 to 8) present slight variations between the two models.

In conclusion, even though there is still lack of knowledge in the literature regarding the outcomes of both resurfacing and stemless shoulder arthroplasties, the results of this study are coherent with previous studies and are expected to provide some clarification about the influence of different shoulder implants on the bone remodelling process of the humerus. Similar levels of bone resorption were observed for the resurfacing and stemless implants. However, the stemless implant lost less density at the implant fixation, which suggests that the stemless implants may be better supported in the long-term, and thus can lead to a better outcome than the resurfacing implants.

## 5. Conclusion

Numerical simulations are valuable tools to predict how bones adapt to different loads after the implantation of a prosthesis, without the need to rely on subjects' dependent clinical trials. In the present work, computational models were developed to study the influence of resurfacing and stemless implants on the process of bone adaptation of the humerus.

The results revealed that the implanted bones were affected by the phenomenon of stress shielding. In particular, a comparison between the intact model and the implanted models revealed similar levels of bone resorption for the resurfacing and stemless implants around the stem and anchor fixation sites, respectively. In addition, for the resurfacing implant, high bone resorption was verified at the region underneath the head cap, indicating unloaded bone stock. Bone apposition was observed around the outer rim of the implants and below the tip of the stem and anchorage fins for the resurfacing and stemless implants, respectively. Nonetheless, the loss of bone density was smaller at the implant fixation of the stemless model, which suggests that stemless implants may be better supported in the long-term than resurfacing implants. For the poor bone quality condition, the loss of bone increased, which supports the limited performance of these implants for reduced bone stock.

Although this study presents a relevant contribution to a better understanding of the process of bone remodelling of the humerus after resurfacing and stemless arthroplasties, future studies should address some of its limitations. For instance, to confirm the results obtained for a single humerus, future works should consider a larger number of humeri. Considering that little is known in the literature about the long-term outcomes of stemless shoulder arthroplasty, it would be interesting to compare the bone adaptation process for different stemless implants, given the distinctive differences that exist in design. Additionally, other critical factors, such as stability, also need to be studied. Subsequent studies may evaluate the stability of the implant after the bone remodelling process in order to understand what are the consequences of the loss of bone density in the long-term support of the implant.

## References


Behrens, B., Nolte, I., Wefstaedt, P., Stukenborg-colsman, C., Bouguecha, A., & Modeling, A. (2009). Finite Element Analysis of Bone Remodeling after Hip Resurfacing Arthroplasty *1*(1):2288–2291.

Bohsali, K. I., Bois, A. J., & Wirth, M. A. (2017). Complications of Shoulder Arthroplasty. The Journal of Bone and Joint Surgery-American Volume *99*(3):256–269.

Burgess, D. L., McGrath, M. S., Bonutti, P. M., Marker, D. R., Delanois, R. E., & Mont, M. A. (2009). Shoulder Resurfacing. The Journal of Bone and Joint Surgery-American Volume *91*(5):1228–1238.

Chan, A. (2014). Biomechanical analysis of the influence of different tibial tray designs in TKA. Instituto Superior Técnico.

Churchill, R. S. (2014). Stemless shoulder arthroplasty: Current status. Journal of Shoulder and Elbow Surgery *23*(9):1409–1414.

Churchill, R. S., & Athwal, G. S. (2016). Stemless shoulder arthroplasty—current results and designs. Current Reviews in Musculoskeletal Medicine *9*(1):10–16.

Coley, B., Jolles, B. M., Farron, A., & Aminian, K. (2008). Arm position during daily activity. Gait and Posture *28*(4):581–587.

Coley, B., Jolles, B. M., Farron, A., & Aminian, K. (2009). Detection of the movement of the humerus during daily activity. Medical and Biological Engineering and Computing *47*(5):467–474.

Dassault. (2012). ABAQUS User's Manual. ABAQUS/CAE User's Manual.

DePuy. (2004). Surgical technique - Resurfacing Humeral Head Implant. England: DePuy International Ltd.

Eberle, S., & Augat, P. (2007). Preventing Contact Convergence Problems in Bone - Implant Contact Models. In *ANSYS Conference 25th CADHEM Users Meeting 2007* (pp. 21–25). Dresden.

Favre, P., & Henderson, A. (2016). Prediction of stemless humeral implant micromotion during upper limb activities. Clinical Biomechanics *36*:46–51.

Favre, P., Snedeker, J. G., & Gerber, C. (2009). Numerical modelling of the shoulder for clinical applications. Philosophical Transactions of the Royal Society A: Mathematical, Physical and Engineering Sciences *367*(1895):2095–2118.

Fernandes, P. R., Folgado, J., Jacobs, C., & Pellegrini, V. (2002). A contact model with ingrowth control for bone remodelling around cementless stems. Journal of Biomechanics *35*(2):167–176.

Fernandes, P., Rodrigues, H., & Jacobs, C. (1999). A Model of Bone Adaptation Using a Global Optimisation Criterion Based on the Trajectorial Theory of Wolff. Computer Methods in Biomechanics and Biomedical Engineering *2*(2):125–138.

Folgado, J., Fernandes, P. R., Guedes, J., & Rodrigues, H. (2004). Evaluation of osteoporotic bone quality by a computational model for bone remodeling. Computers & Structures *82*(17–19):1381–1388.

Geraldes, D. M., Modenese, L., & Phillips, A. T. M. (2016). Consideration of multiple load cases is critical in modelling orthotropic bone adaptation in the femur. Biomechanics and Modeling in Mechanobiology *15*(5):1029–1042.

Gupta, S., & Dan, P. (2004). Bone geometry and mechanical properties of the human scapula using computed tomography data. Trends Biomater Artif Organs *17*(2):61–70.

Gupta, S., New, A. M. R., & Taylor, M. (2006). Bone remodelling inside a cemented resurfaced femoral head *21*:594–602.

Nagels, J., Stokdijk, M., & Rozing, P. M. (2003). Stress shielding and bone resorption in shoulder arthroplasty. Journal of Shoulder and Elbow Surgery *12*(1):35–39.

Netter, F. H. (2006). Atlas of Human Anatomy (Fourth). Saunders/Elsevier.

Ong, K. L., Kurtz, S. M., Manley, M. T., Rushton, N., Mohammed, N. A., & Field, R. E. (2006). Biomechanics of the Birmingham hip resurfacing arthroplasty. The Journal of Bone and Joint Surgery. British Volume *88–B*(8):1110–1115.

Pal, B., & Gupta, S. (2011). The effect of primary stability on load transfer and bone remodelling within the uncemented resurfaced femur. Proceedings of the Institution of Mechanical Engineers. Part H, Journal of Engineering in Medicine *225*(6):549–561.

Poelert, S., Valstar, E., Weinans, H., & Zadpoor, A. A. (2013). Patient-specific finite element modeling of bones. Proceedings of the Institution of Mechanical Engineers, Part H: Journal of Engineering in Medicine *227*(4):464–478.

Quental, C. (2013). Biomechanical tools for the analysis of the native and prosthetic shoulders. Instituto Superior Técnico.

Quental, C., Fernandes, P. R., Monteiro, J., & Folgado, J. (2014). Bone remodelling of the scapula after a total shoulder arthroplasty. Biomechanics and Modeling in Mechanobiology *13*(4):827–838.

Quental, C., Folgado, J., Fernandes, P. R., & Monteiro, J. (2012). Bone remodelling analysis of the humerus after a shoulder arthroplasty. Medical Engineering and Physics *34*(8):1132–1138.

Quental, C., Folgado, J., Fernandes, P. R., & Monteiro, J. (2014). Subject-specific bone remodelling of the scapula. Computer Methods in Biomechanics and Biomedical Engineering *17*(10):1129–1143.

Quilez, M. P., Seral, B., & Pérez, M. A. (2017). Biomechanical evaluation of tibial bone adaptation after revision total knee arthroplasty: A comparison of different implant systems. PLOS ONE *12*(9):1–14.

Razfar, N., Reeves, J. M., Langohr, D. G., Willing, R., Athwal, G. S., & Johnson, J. A. (2015). Comparison of proximal humeral bone stresses between stemless, short stem , and standard stem length: a finite element analysis. Journal of Shoulder and Elbow Surgery *25*(7):1076–1083.

Rothstock, S., Uhlenbrock, A., Bishop, N., Laird, L., Nassutt, R., & Morlock, M. (2011). Influence of interface condition and implant design on bone remodelling and failure risk for the resurfaced femoral head. Journal of Biomechanics *44*(9):1646–1653.

Ruben, R. B., Fernandes, P. R., & Folgado, J. (2012). On the optimal shape of hip implants. Journal of Biomechanics *45*(2):239–246.

Santos, L., Romeu, J. C., Canhão, H., Fonseca, J. E., & Fernandes, P. R. (2010). A quantitative comparison of a bone remodeling model with dual-energy X-ray absorptiometry and analysis of the inter-individual biological variability of femoral neck T-score. Journal of Biomechanics *43*(16):3150–3155.

Schmidutz, F., Agarwal, Y., Müller, P. E., Gueorguiev, B., Richards, R. G., & Sprecher, C. M. (2014). Stress-shielding induced bone remodeling in cementless shoulder resurfacing arthroplasty: A finite element analysis and in vivo results. Journal of Biomechanics *47*(14):3509–3516.

Sharma, G. B., Debski, R. E., McMahon, P. J., & Robertson, D. D. (2010). Effect of glenoid prosthesis design on glenoid bone remodeling: Adaptive finite element based simulation. Journal of Biomechanics *43*(9):1653–1659.

Sharma, G. B., & Robertson, D. D. (2013). Adaptive scapula bone remodeling computational simulation: Relevance to regenerative medicine. Journal of Computational Physics *244*:312–320.

Sobocinski, M. (2015). Analysis of biobearings friction and wear processes. Journal of Applied Mathematics and Computational Mechanics *14*(2):103–109.

Spitzer, V., Ackerman, M. J., Scherzinger, a L., & Whitlock, D. (1996). The visible human male: a technical report. Journal of the American Medical Informatics Association *3*(2):118–130.

Suárez, D. R., Weinans, H., & Van Keulen, F. (2012). Bone remodelling around a cementless glenoid component. Biomechanics and Modeling in Mechanobiology *11*(6):903–913.

Zheng, M., Zou, Z., Bartolo, P. J., Peach, C., & Ren, L. (2017). Finite element models of the human shoulder complex : a review of their clinical implications and modelling techniques. International Journal forNumerical Methods inBiomedicalEngineering *33*(2):e02777.

Zimmer. (2012). Sidus Stem-Free Shoulder - Surgical Technique. Zimmer.